Journal of Bionic Engineering
https://doi.org/10.1007/s42235-022-00208-x

RESEARCH ARTICLE

Multi-material Bio-inspired Soft Octopus Robot for Underwater Synchronous Swimming

Faheem Ahmed[1] · Muhammad Waqas[2,3] · Bushra Shaikh[2] · Umair Khan[2] · Afaque Manzoor Soomro[1,2,3] · Suresh Kumar[1] · Hina Ashraf[4] · Fida Hussain Memon[1] · Kyung Hyun Choi[1]

Received: 9 February 2022 / Revised: 14 April 2022 / Accepted: 19 April 2022

Abstract
Inspired by the simple yet amazing morphology of the Octopus, we propose the design, fabrication, and characterization of multi-material bio-inspired soft Octopus robot (Octobot). 3D printed molds for tentacles and head were used. The tentacles of the Octobot were casted using Ecoflex-0030 while head was fabricated using relatively flexible material, i.e., OOMOO-25. The head is attached to the functionally responsive tentacles (each tentacle is of 79.12 mm length and 7 void space diameter), whereas Shape Memory Alloy (SMA) muscle wires of 0.5 mm thickness are used in Octobot tentacles for dual thrust generation and actuation of Octobot. The tentacles were separated in two groups and were synchronously actuated. Each tentacle of the developed Octobot contains a pair of SMA muscles (SMA-α and SMA-β). SMA-α muscles being the main actuator, was powered by 9 V, 350 mA power supply, whereas SMA-β was used to provide back thrust and thus helps to increase the actuation frequency. Simulation work of the proposed model was performed in the SolidWorks environment to verify the vertical velocity using the octopus tentacle actuation. The design morphology of Octobot was optimized using simulation and TRACKER software by analyzing the experimental data of angle, displacement, and velocity of real octopus. The as-developed Octobot can swim at variable frequencies (0.5–2 Hz) with the average speed of 25 mm/s (0.5 BLS). Therefore, the proposed soft Octopus robot showed an excellent capability of mimicking the gait pattern of its natural counterpart.

Keywords Bio-inspired · Octopus · Octobot · Sub-surface · Soft robotics · Swimming

1 Introduction

For improved human–robot interaction and usefulness of the robots outside of the industrial environment, the robots must be robust, adaptable to variety of environments, and reachable to various types of rough environments. Nature presents enormous number of such creatures who possess the above-mentioned attributes. Such attributes help them to remain safe and survive through the toughest situation. Researchers have put reasonable efforts in designing and development of various soft robots inspired from the natural beings. Soft robots unlike the conventional hard robots use the compliant materials for the robot parts. It is widely considered for different applications in a variety of areas like robotic muscles, climbing robots, edible robots, wearable robots, and prosthetic robots. Soft robots operate in a safe way, often outperforming rigid-link robots in safety [1–4].

As in literatures, many complained that structured robots have been developed to date which interact with unknown environment using the unique features of compliant materials which also is a multi-disciplinary field and referred to as robo-physics [5–7]. Among many, some of the recent studies in this field are micro/millimeter-scale devices which offered the satisfactory demonstration in terms of environmental adoptability and better reachability. The

✉ Muhammad Waqas
mwaqas@iba-suk.edu.pk

✉ Afaque Manzoor Soomro
afaquemanzoor@gmail.com

✉ Kyung Hyun Choi
amm@jejunu.ac.kr

[1] Department of Mechatronics Engineering, Jeju National University, Jeju 63243, South Korea

[2] Department of Electrical Engineering, Sukkur IBA University, Airport Road, Sukkur 65200, Sindh, Pakistan

[3] Advanced Micro Mechatronics and Energy Lab, Sukkur IBA University, Sukkur 65200, Pakistan

[4] Department of Ocean Sciences, Jeju National University, Jeju 63243, South Korea

Published online: 17 May 2022

gait patterns for these devices include crawling, jumping, swimming, and hopping, etc. Unluckily these robots did not exhibit the robustness in terms of shape changing since they used non-compliant or partially rigid parts. In the same way, dielectric elastomer-based swimming fish was designed which mimicked the undulating motion approach demanding higher voltage up to 3 kV for locomotion [8]. Additionally, all of the soft robots creating bio-inspired systems that are able to walk, crawl, jump, roll or swim [9–11] fall under one actuation methods used for soft robots such as fluidic actuation [2, 12, 13], which uses pressurized fluids and fluid filled chambers, dielectric elastomer actuation [14–17] that work based on the induction of deformation due to electric field, pneumatic actuation [8, 18–20] and it utilizes the air pressure to actuate, SMA-based actuation [21–23] which makes use of memory feature of the SMA wire. Actuation methodologies also contain magnetorheological, and Shape Memory Polymer (SMP)-based actuation techniques.

Recently, soft robotics has focused on new and demanding paradigm of underwater exploration and monitoring using biomimetic actuators which paved the way for simple structured robots equipped with better adoptability, efficiency, and reachability [5, 6, 24]. This was achieved by mimicking the morphology of natural creatures as closely as possible by approximating their natural gait patterns with theoretically infinite degree of freedom offered by soft actuators [7, 25, 26]. The detailed underwater exploration and monitoring was made possible by the design of the underwater robots along with better understanding and interpretation of biomechanics and close control of underwater creatures [27, 28]. One of the recent studies on design concepts and kinematic model for soft aquatic robot is given in [29]. In the mentioned study, kinematic model is developed to characterize the motion which enables precise position feedback using strain gauges. Additionally, another study is done in [30] which presents a flexible-bodied underwater glider. A robust hydrodynamic shape for the vehicle under the internal liquid pressure is achieved with the help of flexible covering. To verify the performance of motion characteristics, sea trials were conducted. The results demonstrated that the as-developed flexible-bodied glider performs better in practice. Furthermore, with the help of underwater soft robots, researcher can record and analyze the tiny details and closely monitor the natural behaviors of underwater species. Because capturing good-quality images and videos underwater can help scientist discover many realities and the response of the underwater species would be real when interacting with biomimetic soft robot [31]. In addition, for designing a robot for underwater monitoring is quite challenging since it involves many things like water mechanics, fluid–solid interactions and propulsion mechanism for enhanced robustness and improved performance of the soft robot [28, 30, 31]. Among vast number of underwater species, octopus presents effective trait of being completely soft creature possessing the attributes like better reachability and adoptability [32, 33]. The mechanism which octopus follows for swimming is quite different from the other marine species. It creates the thrust by expelling a jet of water from the mantle through its siphons. It also possesses the property of contracting and expanding its muscles to fit in the irregular and undetermined environment. In the past, much efforts have been made to mimic the morphology of the octopus and one such study is present in [34]. The study mainly focused on to achieve the actuation of octopus tentacle using the SMA springs in the tentacles of the octopus. Most of the studies are based on hard systems like gears and motors, which leaves a space for robots that should be completely compliant and effectively mimicking the morphology of the real octopus.

In this paper, the locomotion and gait pattern of the octopus for obtaining the synchronous swimming was gained using the antagonistic SMA muscle wires (SMA-α and SMA-β) which actuate at 70 ^{0}C for actuations, Ecoflex-0030 [35] having shore hardness level of 5 [36] for casting the Soft Octobot tentacles, and OOMOO-25 for casting head of Octobot. The design of the molds for Octobot was made in 3D designing software called SolidWorks 2018. Each of the 8 tentacles having the length of 80 mm and diameter of 8 mm was casted using the 3D molds (Fig. S2) in four steps. First, molds were designed, and 3D printed, second the compliant material was prepared and casted for 2 h, third SMA Antagonistic muscle wires (BMF 150) were trained to required shape, and forth, the trained SMA muscle wires were installed followed by full curing of the compliant tentacle material as shown in Fig. 1a–d respectively. Octobot head is simply casted using the dye shown in Fig. S2. Additionally, rigorous simulation work is done for analyzing the surface velocity generated by the locomotion of the Octobot tentacles in two sets (each set contains four tentacles) and strain produced due to contraction and expansion SMA muscle wires. It was ensured that the proposed design effectively copied the natural octopus gait pattern. The, here developed, Octobot was controlled by pulse width modulation signal using Arduino nano which is programmed through in-house made LabVIEW software. The PWM pulse applied through LabVIEW custom-made software heats the SMA muscle wire up to 70 °C causing the locomotion of the Octobot tentacle for thrust generation as shown in Fig. 1e. To bring the SMA muscle (SMA-α) back, another SMA muscle wire called SMA-β is installed to provide antagonistic mechanism alongside the natural cooling process. Following the antagonistic mechanism, the Octobot successfully demonstrated the synchronous swimming at controllable frequencies ranging from 0.5 to 2 Hz.

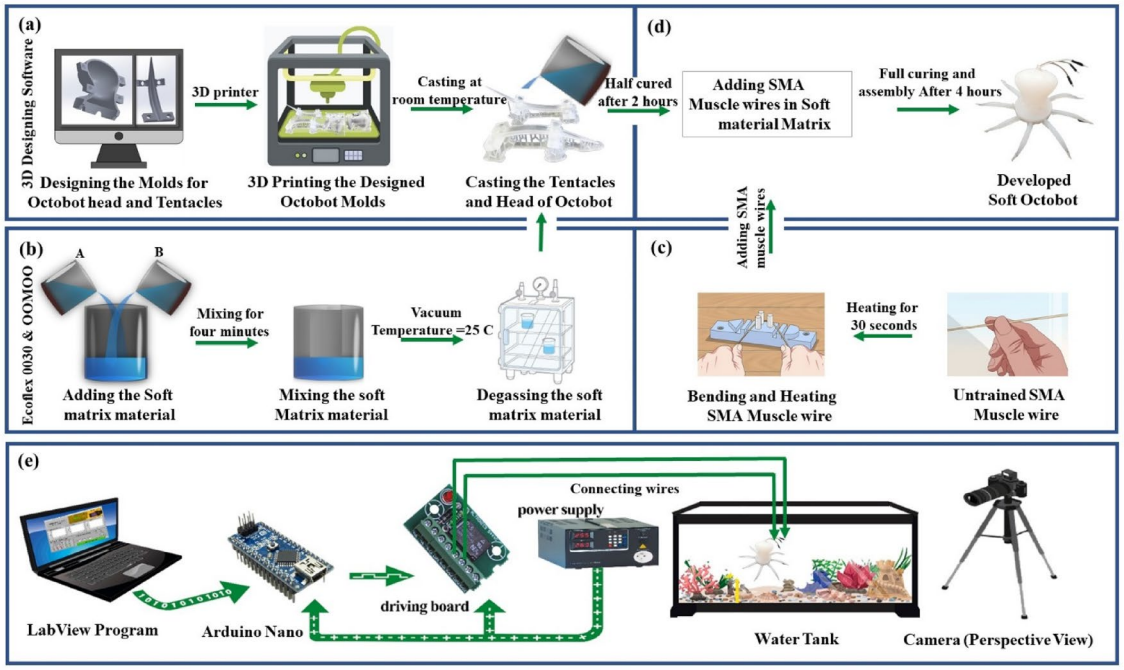

Fig. 1 **a** Designing using the 3D designing software followed by 3D printing of the molds in parts, such as the Octobot tentacle and the head, are designed in two parts each, **b** preparing the Ecoflex-0030 for casting Octobot tentacles, whereas preparing the OOMOO-25 for casting head, **c** after that heat is applied for training the SMA Muscle wires for required shape, **d** casting and installing trained muscle wires in Octobot tentacles, **e** in-house-built LabVIEW software for monitoring and control of the Octobot

2 Experimental

Experiments for the Octobot were performed in in-house built experimental set-up. The set-up consisted of the transparent tank made of glass having volume equal to 0.3 m × 1 m × 0.5 m which was filled with water, camera for rare view, and power supply system etc. For enhanced stability of the robot, apart from the design aspect, wire connections were carefully considered. The cyclic actuations of the SMA muscle wires were performed by providing the PWM pulse generated through the Arduino nano controller and directly controlled through in-house made software based on LabVIEW as shown in Fig. 1e. The Octobot tentacles are divided into two groups. Each group contains four tentacles. The first group is actuated and as soon as the PWM pulse is stopped to first group, second group is actuated to provide the continuous actuation for continuous thrust. Additionally, the further detailed description of the working mechanism of the Octobot is shown in Fig. 2. Since the current required for the each SMA muscle wire was up to 350 mA which cannot be directly provided by the Arduino alone. Hence, an H-bridge circuit was used to provide the PWM pulse of 350 mA current, whereas the circuit was controlled by the Arduino nano. The signal of 9 V and 350 mA was applied to every SMA muscle for actuation. For monitoring perspective views, a camera was provided which recorded the data. The software was custom-made in LabVIEW which served two purposes. First, it worked as monitoring software for real-time actuation, strain, force and tentacles monitoring; second it worked as controlling software to control the frequency, voltage and number of actuation cycles during the experiment.

2.1 Fabrication Process

The soft Octobot was designed using the process of soft molding and casting. The molds were designed in SolidWorks 2018, a 3D designing software. The drawings for the molds design are shown in Fig. S3. The drawing dimensions clearly show that, the diameter void space of the tentacle is 7 mm, and the length of void space is 79.12 mm, whereas, the overall length of the tentacle is 93.51 mm. All the eight tentacles are produced using only one mold. The procedure is similar to one that is followed in [37]. The head and tentacles of the Octobot were designed separately while each of the head and tentacle was made in two parts upper and lower. For tightening of two parts during the casting process, molds were provided with screws on the sides as shown in Fig. S3. Molds were 3D printed with ABS filament (BLACKMAGIC3D, 1.75 mm) transparent material using "ANYCUBIC

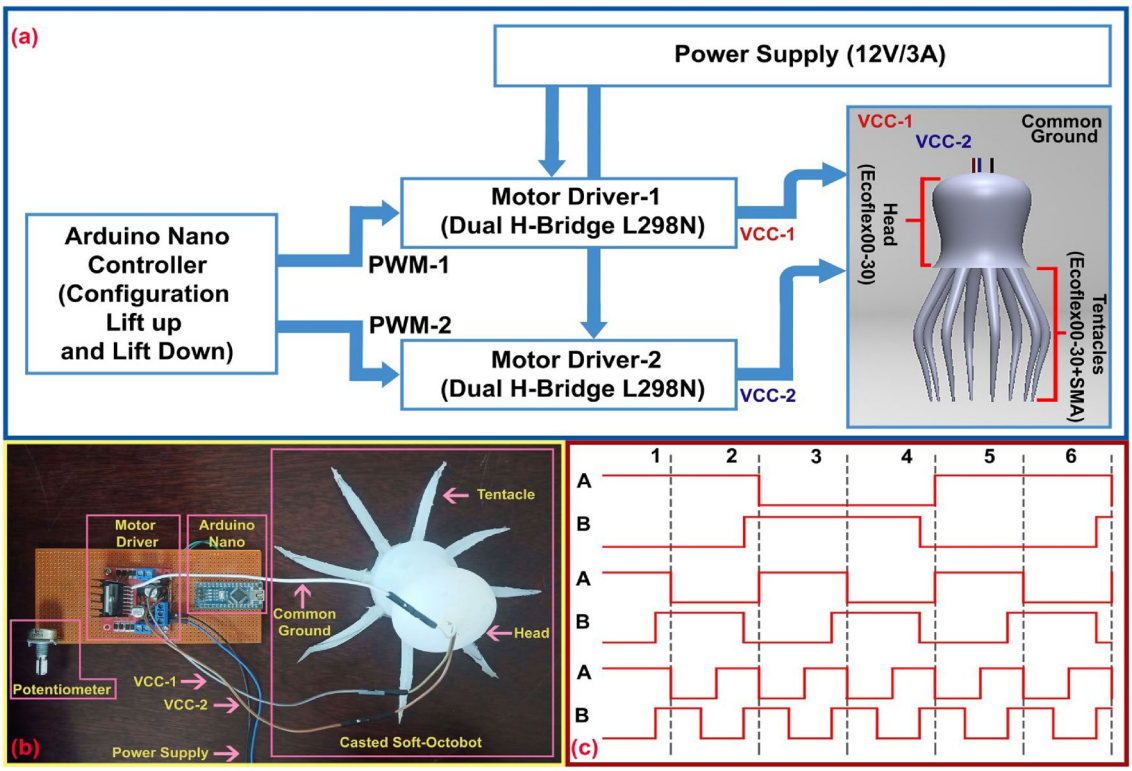

Fig. 2 Working mechanism of the Soft Octobot, **a** controller diagram for Octobot showing the layout of the control and flow of PWM pulses along with the tags of the components used and **b** the prototype demonstration of the Octobot set-up and PWM pulses for alternative leg groups

Mega S Upgrade FDM 3D Printer" with the help of Fablab academy Khairpur, Pakistan. All the printing processes were done two steps. In first step, lower part of head and tentacle; and in second step, upper part of head and tentacle was printed. The printed molds are shown in Fig. S2. Moreover, the casting process was completed in three steps. First, the compliant material was prepared by mixing for 5 min followed by degasification and then casting for 2 h, second SMA Antagonistic muscle wires (BMF 150) were trained to required shape, and third, the trained SMA muscle wires were installed followed by full curing of the compliant tentacle material as shown in Fig. 1b–d respectively. Additionally, the individual tentacles with embedded SMA muscles and assembled Octobot are shown in Fig. S4 (a–b) respectively.

SMA muscle wire serves as a foundation for the actuation of the Octobot. In this connection, it is necessary to ensure its essential characteristics. The SMA muscle wire (diameter 0.5 mm) was purchased from (Shanghai Metal). It is used for main thrust force generation and for providing the antagonistic movement for the tentacles of the Octobot. SMA wires show contraction when exposed to heat or increased temperature. The modes of SMA can be classified into two categories: martensite and austenite. When the temperature is increased to certain range the SMA muscle wire shifts from martensite to austenite demonstrating the contraction. In our experiment, we have used electric current to provide stimulant for SMA to actuate by changing its temperature. As a result, thrust force is generated from contraction of the SMA. To test the muscle for experiment, we conducted another experiment with load (50 g) attached to the middle with spring. The wire was then heated while the temperature was continuously monitored using pyrometer gun. Voltage (7.0–9.0 V) and current (50–300 mA) and temperature (60–200 °C) were changed with predefined step sizes. Similarly, the resistance of SMA was measured at various contracting strains (0–0.35%) using Agilent E3634A, electric current flowing at different temperature values was also measured. This was of great help in controlling the power consumption of the SMA using our custom-developed software.

3 Results and Discussion

3.1 Simulation of Octobot

For characterization of the developed robot working principle and its design, simulation was conducted in SolidWorks Software. Non-linear solid mechanic simulation loads generated by advanced features of the computing tools were

imported in SolidWorks fluidic environment for simulation to generate the synchronous motion which basically caused the Octobot to swim [38–40]. The fluidic environment set is shown Fig. S5 (a). Similarly, the Octobot model being simulated in the SolidWorks simulation environment is shown in Fig. S5 (b). For the synchronous motion simulation deep, non-linear features of the SolidWorks from solid mechanics and fluidic environment were used [39, 40]. In addition, dynamic characteristic model having multiple input–output (MIMO) was developed for performing the simulation work of the Octobot [40]. The basis for MIMO was the grouping of Octopus tentacles in two groups (A and B) where each group consisted of four tentacles. The essential parameters of the Octopus synchronous swimming pattern, such as displacement, lift, drag, and velocity, were taken into account. Since the synchronous swimming motion demonstrated by the Octobot is the result of combined effort of the tentacles of the Octobot and the fluid which encouraged the implementation of the meshing and remeshing for simulating the complex simulation pathways. The simulation was carried out in 3D environment, and the simulation was carried out in batches for each group of tentacles. The simulation was directed from downward to upward to closely mimic the swimming pattern of the real octopus and the method we have mimicked in our Octobot. The simulation video (shown in SMOVIE1) demonstrates the surface velocity and thermal load distribution across the tentacles in the SMA muscles along with the batchwise actuation of the tentacles.

Since the bioinspired soft robots are made of compliant materials, so the lift-and-drag force generated plays key role in determining the overall performance of the bioinspired robots. In this connection, the force distribution was calculated in simulation as well as in practical. The practical distribution is shown in Fig. 5c. However, Fig. 3 shows the series of images taken from the simulation of the Octobot. Each image attached in Fig. 3 shows the surface velocity magnitude in (mm s^{-1}), whereas the time is represented in seconds (s) and the displacement is given in the form of millimeters (mm). The synchronous actuation generated is due to the actuation of tentacle. For each set of tentacles, Fig. 3a shows the actuation of the first four tentacles (Group A) followed by the actuation of the second group of the tentacles (Group B) as shown in Fig. 3b. Collectively both groups A–B (all eight tentacles) constitute towards the locomotion of the Octobot, whereas time-based position of the tentacles recorded through tracker is shown in Fig. 6b. The recorded actuation stroke time is 6 s. Similarly, the instantaneous velocity in x and y direction for the tentacles is shown in Fig. 6e. The peak fold velocity is 40 mm s^{-1} which is twice the velocity of Octobot thigh as shown in Fig. 6f.

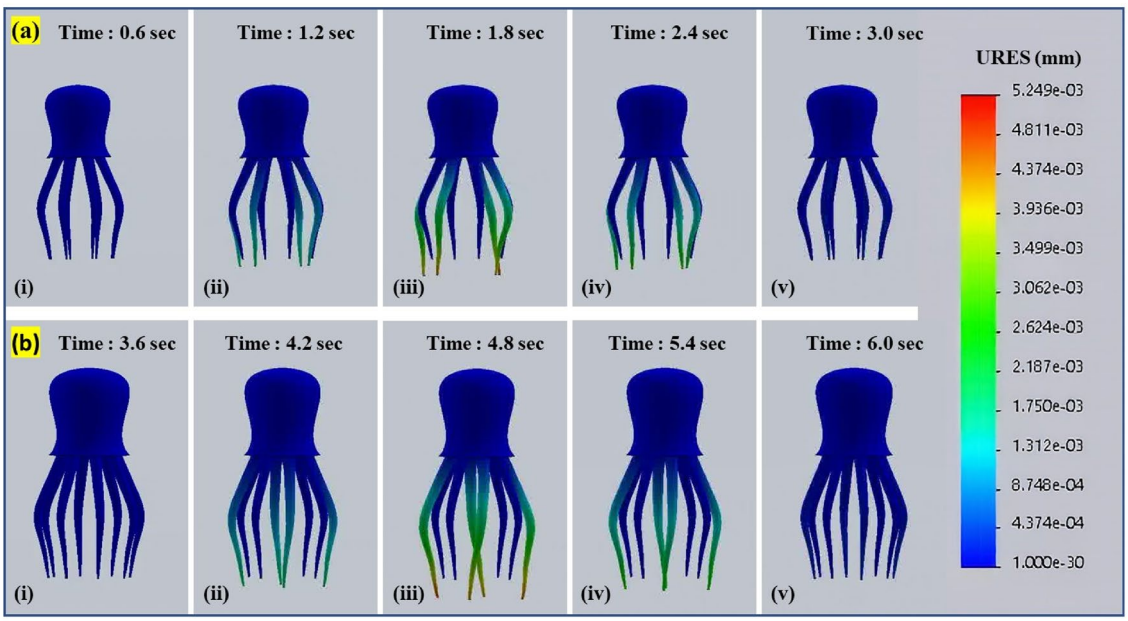

Fig. 3 Figure showing the simulation work of Octobot, whereas the Octobot tentacles are divided into two group and each group contains four tentacles. **a** The first group of tentacles is being actuated as shown and **b** after the PWM pulse is stopped to first group it is being applied to the second group of tentacles being actuated

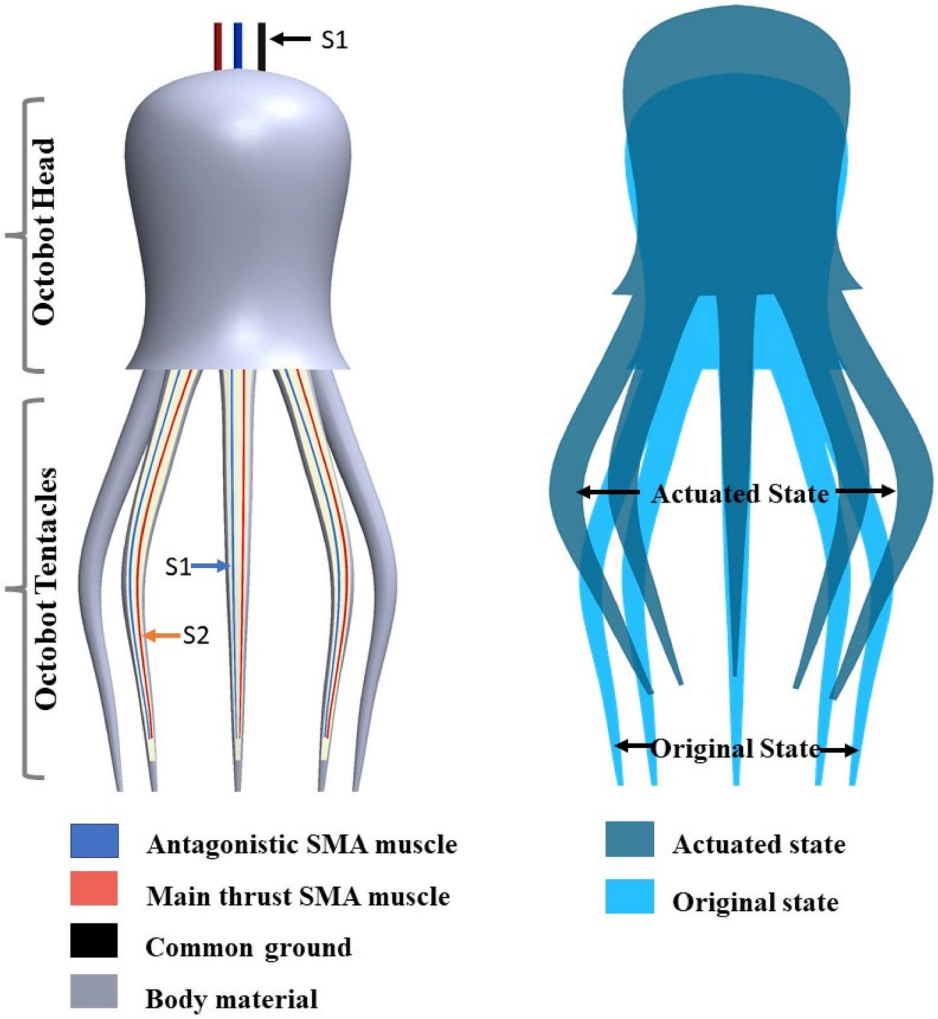

Fig. 4 Complete mechanism of Soft Octobot with complete stroke. On the left side, Octobot along with internal structure is shown. Antagonistic and main thrust wires are shown in blue and red color respectively. The Actuated and the original state of the Octobot are shown on the right side of the figure

As per results of simulation and mathematical modelling, the locomotion of the eight tentacles was achieved based on the thrust generation and antagonistic SMA muscle approach. Each of the tentacle as already reported contains two muscle wires. One mainly generated the thrust for the actuation and the second helped in returning of the actuated tentacles to their first place supported by the compliant nature of the material. The custom-made software (LabVIEW-based) controlled and monitored the actuation of the muscles at specified time by producing PWM pulses for four tentacles alternatively as shown in Fig. 4.

3.2 Mathematical Model

The behavior of the SMA wire is observed under constant load by heating it at the room temperature and the result is hysteresis loop. The length of the SMA wire is changed due to temperature. The Fig. 6S is showing hysteresis loop having two sides upper and lower. The upper side depicts the behavior when the SMA wire is heated, and the lower side depicts when it is cooled down. At low temperature, the curve diverges, and at high temperature, it converges.

$$L(T) = -mT + c, \tag{1}$$

$$m = \frac{Y2 - Y1}{T2 - T1}, \tag{2}$$

$$c = Y1 + aT1. \tag{3}$$

The diagonal length is found using distance formula

$$d = \sqrt{(T2 - T1)^2 + (Y2 - Y1)^2}. \tag{4}$$

The two sides are shown in below Fig. 6S, $y1\ (T)$ and $y2\ (T)$ respectively. We can see half-sine wave which is added to the diagonal straight line:

$$L(T) = c - \mathrm{m}T \pm Aij\sin\theta, \tag{5}$$

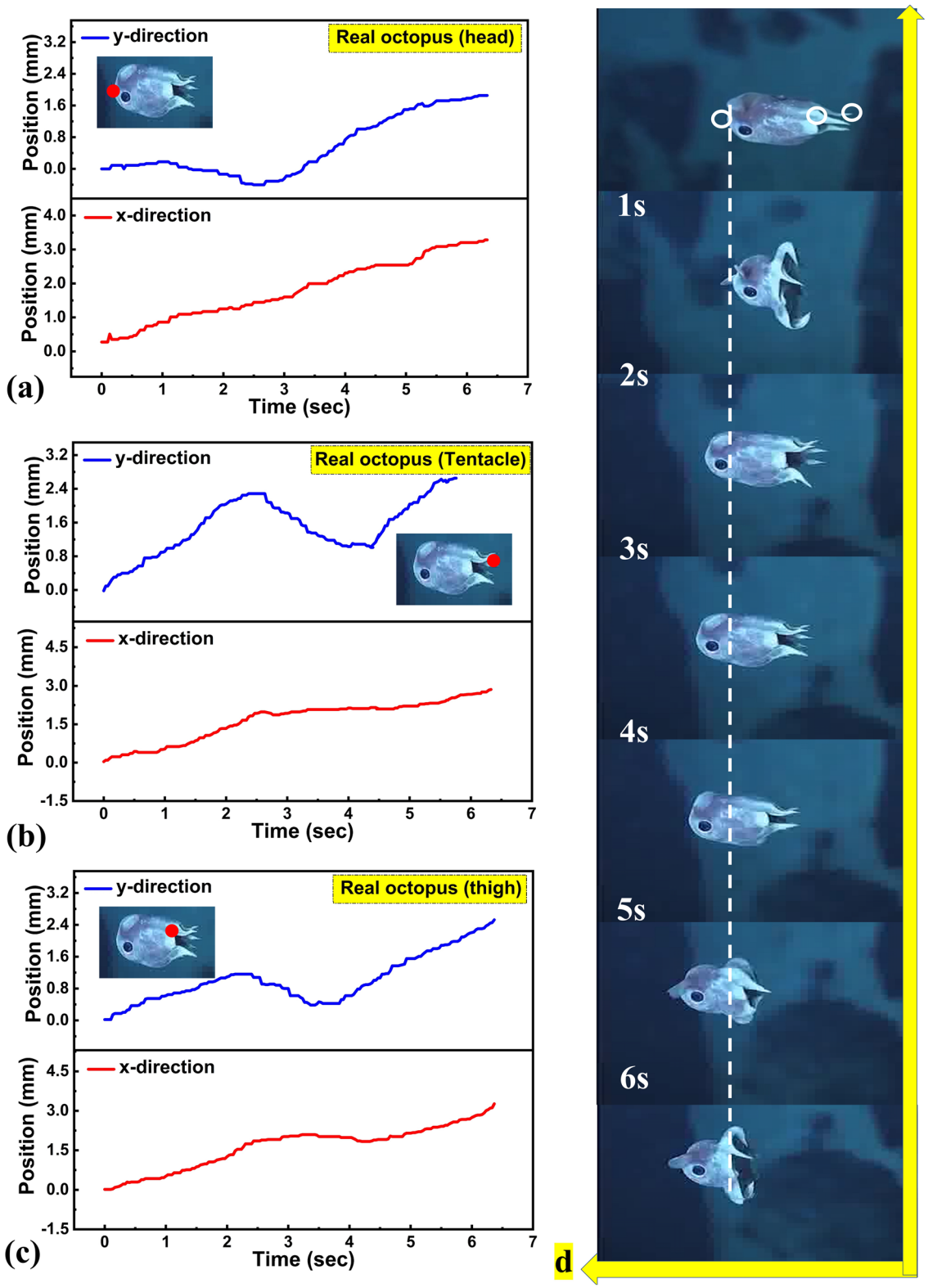

Fig. 5 Real Octopus analysis and positional curves in *x* and *y* directions acquired using the traced points in TRACKER software (a video analysis tool), **a** head point of the octopus, **b** tentacle or the tip of the limb of the octopus, and **c** the thigh point of the tentacle. (Octopus snapshots were recorded after 1 s lapse of time)

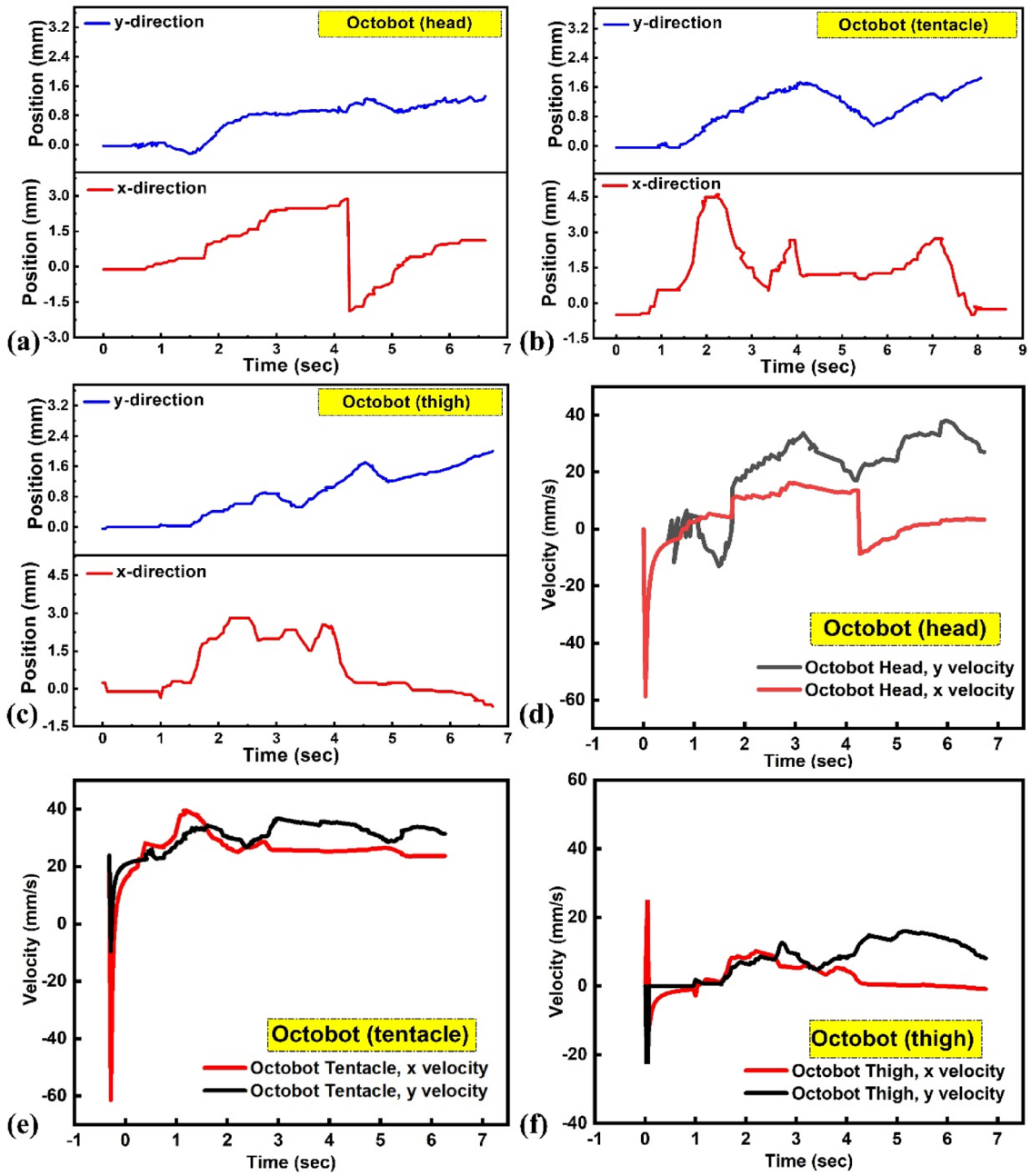

Fig. 6 The analysis of proposed **a**–**c** Octobot and position of head, thighs, and tentacles is tracked using the tracker software after the video is recorded, similarly **c**–**f** instantaneous velocity measured for the Octobot at given locations is also measured through the tracker software

$$A = \left| \frac{y2(Tc) - y1(Tc)}{2} \right| * \cos\alpha, \tag{6}$$

$$Tc = T1 + \frac{T - T1}{L1}. \tag{7}$$

The positive and negative signs represent the upper and lower curves of the SMA. So, the above equation shows the change in length when temperature is applied to the SMA wire. The relation for change in length with respect to temperature individually for upper and lower curves of SMA is found:

$$Lm1(T) = c - mt - A\sin\left(\frac{\pi(T - T1)}{L1}\right) \text{for}\{T1 \le T \le T2\}, \tag{8}$$

$$Lm2(T) = c - \mathrm{m}t - A\sin\left(\frac{\pi(T-T1)}{L2}\right)\text{for}\{T1 \le T \le Tcr\}, \tag{9}$$

$$Lm2(T) = c - \mathrm{m}t - A\sin\left(\frac{\pi(T-T1)}{L21}\right)\text{for}\{Tcr \le T \le T2\}. \tag{10}$$

For more accurate results, tuning coefficient is added.

$$Lm1(T) = c - \mathrm{m}t - U11A\sin\left(\frac{\pi(T-T1)}{L1}\right)\text{for}\{T1 \le T \le T2\}, \tag{11}$$

$$Lm2(T) = c - \mathrm{m}t - U21A\sin\left(\frac{\pi(T-T1)}{L2}\right)\text{for}\{T1 \le T \le Tcr\}, \tag{12}$$

$$Lm2(T) = c - \mathrm{m} - U22A\sin\left(\frac{\pi(T-T1)}{L21}\right)\text{for}\{Tcr \le T \le T2\}, \tag{13}$$

where the T_{cr} is the intersection of upper curve and diagonal and the above mathematical model shows two points ($T1$, $L1$) and ($T2$, $L2$) of the hysteresis. Here, a closed mathematical model is developed, the mathematical model consists of algebraic and trigonometric functions [2, 17].

The Octobot arm is divided into two parts, proximal and distal part. The proximal part is attached to the center of the body of the octopus which is stationary; as for the distal part is concerned, its movement is restricted along the Octobot arm. The modeled model is one-dimensional. Assume, the total force generated by the muscle can be combined into a force (Fm) which is working in the direction of the arm. Moreover, the force of the muscle starts at some initial force (Fi) when the limb moves down the arm will decrease proportionally to the cross-sectional area.

$$Fm = Fi * \frac{A(d)}{A(0)}. \tag{14}$$

Herein d is the position along the arm using Newton's second law of motion,

$$Fm - FD = 2\left(a * m(x) + v^2 * \frac{\mathrm{d}m(x)}{\mathrm{d}x}\right), \tag{15}$$

where v is the velocity of the tentacle and a is the acceleration of the tentacle, where $m(x)$ is the mass of the distal part of the tentacle. Here, FD is the drag force which resists the motion in the water. The drag force opposes the movement of Octobot in the water [18].

$$FD = \frac{1}{2} * \rho * SA * d^2 * \mathrm{Cd}, \tag{16}$$

where, ρ is the density of the fluid, and S_A is the surface area which depends upon the shape of the object. Here the shape is taken the distal part of the limb. And Cd is the dimensional-less drag coefficient which always depends upon the shape of the distal part of the limb [17]:

$$\lambda(s) = \frac{\mathrm{d}m}{\mathrm{d}s}, \tag{17}$$

where $\lambda(s)$ is the longitudinal mass density

$$P = \int_0^l \rho(s) * d(s) = \int_0^l V(s) * \lambda(s) * \mathrm{d}s. \tag{18}$$

P is the momentum equation shown above:

$$V(s) = \begin{cases} 0 & S < d \\ 2d & S \ge d \end{cases}, \tag{19}$$

where V(s) is the velocity at point, the point $s < d$ is assumed to be stationery and $S > d$ is supposed to be the moving point.

The sum of forces is given below:

$$F = \frac{\mathrm{d}}{\mathrm{d}t}\left(\int_0^l V(s) * \lambda(s).\mathrm{d}s\right) = \frac{\mathrm{d}}{\mathrm{d}t}(2 * v * m(d)), \tag{20}$$

$m(d)$ is the distal part mass at position x given by:

$$m(d) = \mathrm{m}t\left(1 - \frac{x}{l}\right)^3, \tag{21}$$

Now, Eq. (20) can be written as:

$$F = 2 * a * m(x) + 2 * v * \frac{\mathrm{d}m(x)}{\mathrm{d}t}. \tag{22}$$

From Eqs. (20) and (22), we get

$$F = 2 * a * m(x) - 6 * \frac{mt}{l}\left(1 - \frac{d}{l}\right)^2 * v^2. \tag{23}$$

So, here presentation of the mathematical model for our Octobot robot that includes the calculation procedure for actuation of SMA along with the fluidic force (drag force) for our Octobot robot.

3.3 Real Octopus Simulation

The motivation that served the basis for the proposal and then development of Octobot was Octopus. Thus, it is important to understand and observe quantitatively and qualitatively swimming patterns that octopus follows. As the observations from the analysis of the real octopus can significantly help in the development of the Octobot from design to final prototype development. To make this happen, a real Octopus video with high-definition quality was download and used for analysis. A heavy computing power machine was utilized for the video analysis and the two-dimensional kinematics were digitized with high framing

rate of 250 frames/s. The specific points on the robot body of the actual Octopus were focused. The elected focused points were head, thigh, and the tentacle of the Octopus. First, automatic tracing was performed using vector points, and second using the direct linear transform, all the linearly automatically traced frames were corrected manually. The application of the DLT ensured the removal of any unwanted error in data. The error median in the data was found to be approximately ~ 0.55 mm. Due to higher video resolution, only one stroke was considered (one stroke for each set of tentacles) for 6 s as shown in Fig. 5a–c. The ultimate target for this analysis was to find out the swimming pattern of the octopus. The displacement in x direction is shown due to slight diversion and the lift-and-drag force generation for the stroke. Instead, the octopus kept moving the direction along y. The octopus head as shown in Fig. 5a is traced along x and y directions like the octopus tentacle and thigh as shown in Fig. 5c. Moreover, Fig. 5 depicts the motion along the y-axis is cyclic since it is the result of the stroke, whereas the distance and motion along x-axis remain reasonably constant. This behavior of the real octopus is observed in the developed Octobot as shown in Fig. 6a–c. However, at the start, the octopus moved behind due to resultant negative force production but then moved to the maximum shown level 3.2 mm in 6th second.

To verify the synchronous swimming of the developed Octobot, a tank made of transparent glass was filled with water to around 80% approximated level of its total volume. The home-made setup was equipped with camera to record the videos and actuation performance of the designed Octobot in real time. An Arduino Nano (Academic) controller was installed in the circuit to produce the controlled PWM pulses of frequency ranging from 0.5 to 2.0 Hz. Speed of the Octobot at different operating frequencies is given in Fig. S6 (c). The frequency range is set from 0.5 to 2.0 Hz while the maximum speed of 25 mm/s is attained at the frequency of 1.5 Hz. The speed of the Octobot after 1.5 Hz starts to decline and 23 mm/s is observed at the frequency of 2.0 Hz. This frequency was set to target the muscle wires (SMA) installed in the tentacles and to boost the current and power. H-bridge motor driver circuit was used in the circuit. Flexible and quite thin, highly conductive copper wires were used for connection and electric current delivery. The minimum negative force, as it was ensured was caused by the connecting wires. The LabVIEW-based custom-made software developed in lab helped in control and real-time monitoring of the Octobot in experimental setup with significant control on each part of the experimental setup [42]. Pyrometer gun was used to measure the temperature as the feedback throughout the experiment. There was significantly linear relationship between temperature applied and current. Moreover, SMA was found destroyed when it was heated more 200 °C. During the experiment, it also resulted in adverse effect to the matrix material of the tentacle, and as a result, it started to melt down. Thus, the set point for the Octobot was made fixed below 100 °C, but due to comparatively lower water temperature (approximately 22 °C), SMA had an additional protection and never found damaged.

Additionally, the simulation and mathematical modeling is similar to the study conducted in [43, 44]. In simulation, first, group A tentacles start to displace and then group B and the cycle goes on. Moreover, the displacement and the strain produced in the SMA muscle wire of 0.3 mm and 0.5 mm diameter have been calculated (Fig. 7a–b), when the wire is heated. Second, the study of the Octobot is conducted and the displacement and strain produced in the tentacles is calculated and plotted for the temperature changes in SMA wire as presented in [45, 46]. Third, the force generated by octopus tentacle [47] is calculated and plotted. The results are shown in Fig. 7. Figure 7a shows higher strain in case of 0.5 mm wire and higher displacement in case of 0.3 mm wire as shown in Fig. 7b. Additionally, the comparison between the actual octopus and developed Octobot mentioned in Fig. S6 (a) shows the position change of the Octobot in x and y direction, whereas Fig. S6 (b) shows the position change of the real octopus in x and y direction. The comparative analysis reveals that Octobot mimics the pattern followed by the real octopus in y-direction. However, there is slight dip in x-direction for the Octobot due to change in x-direction, otherwise it remains considerably stable.

Following the simulation, tentacles of the Octobot are divided in to two groups (A and B) and each group contains four tentacles. Initially, group A tentacles are actuated by applying the PWM pulse for a given period (determined by the operating frequency) and once the PWM supply is cut to group A, at the same time, it is applied to group B tentacles. This continuous periodical actuation of the tentacles helps achieve the Octobot maximum speed of 25 mm/s as shown in Fig. 8. Moreover, the high-definition camera device was used to capture the images of the swimming experiment of Octobot, as shown in Fig. 8. The total recorded duration of the Octobot is 6 s and the images are taken at the fix time step of 0.6 s each. The images at the fixed interval of time are showing the movement of Octobot tentacles and finally helping it lift upward. Initially, until 1.2 (Fig. 8ai–ii) seconds, there is no significant movement in the tentacles, but at the time of 1.8 s, the Octobot tentacles are actuated and the Octobot is trying to move upward due to thrust generated by the group (4 tentacles) being actuated at the same time (Fig. 8aiii–x). Finally, targeted applications of the developed Octobot are underwater maintenance and monitoring applications, such as underwater pipe inspection, repair of offshore infrastructure. Biological applications of the designed robot are seabed and abyssal exploration, sample gathering from marine or sub-surface environment, such as coral reefs and data collection.

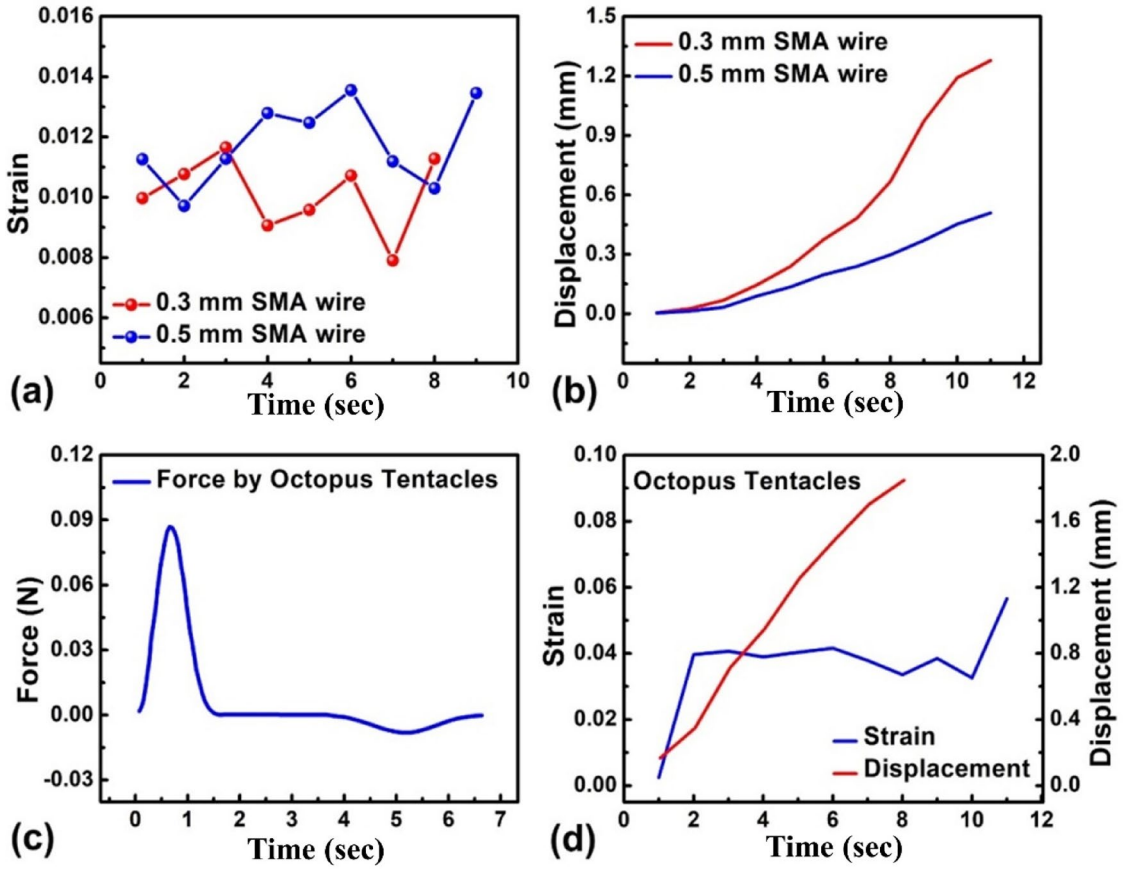

Fig. 7 **a**, **b** The graphs for strain and displacement produced in SMA wires of 0.3 mm and 0.5 mm diameter are shown. In **c**, **d** the graph for force of the octopus's model and strain produced in octopus tentacles are given respectively

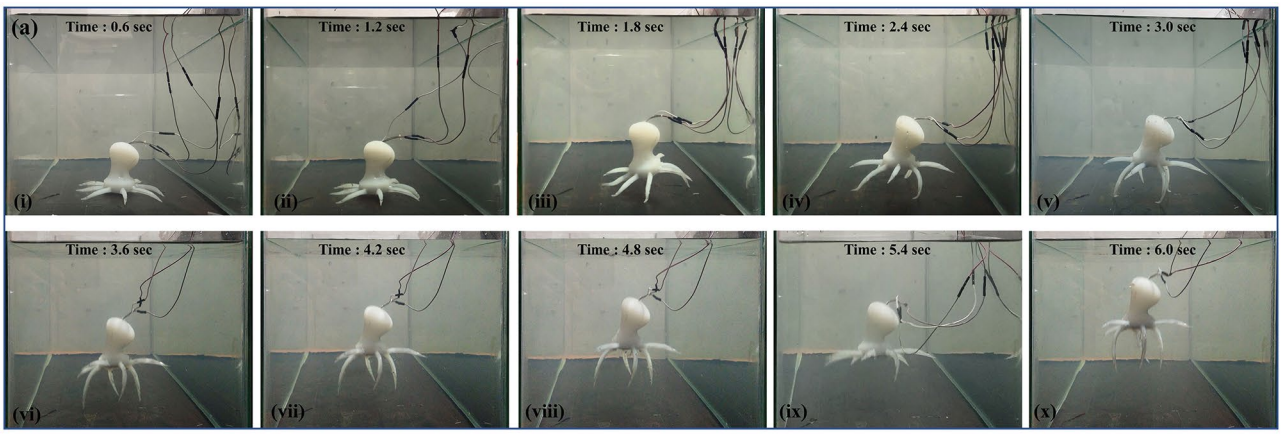

Fig. 8 Images taken from the synchronous swimming experiment of Octobot; i–v) are showing the actuation of the first four tentacles of the Octobot (Group A) under applied PWM pulse, whereas, vi–x) are similarly showing the actuation of the Group B tentacles when the PWM pulse is stopped to Group A and applied to Group B. The sequential pictures taken at the fixed time step size

4 Conclusion

This work presents soft Octopus robot (OCTOBOT), specially designed for synchronous underwater swimming. Entirely soft Octobot was fabricated after its design optimization using mathematical modelling, behavioral simulation analysis, and focusing on the morphology of the real Octopus. Tracker software was used to analyze the motion of the real Octopus. The developed model is governed by the mathematical analysis along with simulation work carried out in SolidWorks 2018 for the verification of the design and working mechanism. Following simulated model, the Soft Octobot was developed using molding and casting process. The material for the molds was ABS, whereas for the casting, Ecoflex 00-30 (For tentacles) and OOMOO-25 (For head) were used. The functionally responsive tentacles were attached to the head of the Octobot. The length of each tentacle was 79.12 mm and 7 mm void space diameter. The basic thrust generation was made possible with the help of SMA muscle wire (BMF 150) along with additive functionality of the antagonistic muscle with flexible matrix material significantly improved the frequency up to 0.5–2.0 Hz. Furthermore, real environment was mimicked for the Octobot, such as transparent water tank was filled with water to witness the performance and synchronous swimming of the 25 mm s^{-1} at the given frequency of 1 Hz, 300 mA current and 9 V. The designed soft Octobot can be a strong candidate in the list of soft bio-inspired robots designed for underwater monitoring.

Supplementary Information The online version contains supplementary material available at https://doi.org/10.1007/s42235-022-00208-x.

Acknowledgements This work was supported by the National Research Foundation of Korea (NRF) Grant funded by the Korea government (MSIT) (NRF-2022R1A2C2004771) and Internal Research Grant by ORIC, Sukkur IBA University 2022.

Data availability statement Data available on request from the authors.

Declarations

Conflict of interest The authors declare no conflict of interest.

References

1. Stilli, A., Grattarola, L., Feldmann, H., Wurdemann, H. A., & Althoefer, K. (2017). Variable stiffness link (VSL): Toward inherently safe robotic manipulators. In *Proceedings—IEEE international conference on robotics and automation*, *Singapore* (pp. 4971–4976). https://doi.org/10.1109/ICRA.2017.7989578
2. Fras, J., Noh, Y., Macias, M., Wurdemann, H., & Althoefer, K. (2019). Bio-inspired octopus robot based on novel soft fluidic actuator. In *Proceedings—IEEE international conference on robotics and automation*, *Brisbane, Australia, 2018* (pp. 1583–1588). https://doi.org/10.1109/ICRA.2018.8460629
3. Soomro, A. M., Fida, H., Jae-Wook Lee, A., Faheem, K. H., Kim, K. YSu., & Choi, K. H. (2021). Fully 3D printed multi-material soft bio-inspired frog for underwater synchronous swimming. *International Journal of Mechanical Sciences*. https://doi.org/10.1016/j.ijmecsci.2021.106725
4. Soomro, A. M., Khalid, M. A. U., Shah, I., Kim, S. W., Kim, Y. S., & Choi, K. H. (2020). Highly stable soft strain sensor based on Gly-KCl filled sinusoidal fluidic channel for wearable and waterproof robotic applications. *Smart Materials and Structures,* 29, 25001. https://doi.org/10.1088/1361-665X/ab540b
5. Shintake, J., Cacucciolo, V., Shea, H., & Floreano, D. (2017). Soft biomimetic fish robot made of dielectric elastomer actuators. *Soft Robotics, 5*(4), 466–474. https://doi.org/10.1089/soro.2017.0062
6. Sfakiotakis, M., Lane, D. M., & Davies, J. B. C. (1999). Fish swimming techniques. *IEEE Journal of Oceanic Engineering, 24*(2), 237–252. 0364-9059(99)03032-0.
7. Ulloa, C. C., Terrile, S., & Barrientos, A. (2020). Soft underwater robot actuated by shape-memory alloys 'jellyrobcib' for path tracking through fuzzy visual control. *Applied Sciences*, *10*, 7160. https://doi.org/10.3390/app10207160
8. Wehner, M., Truby, R. L., Fitzgerald, D. J., Mosadegh, B., Whitesides, G. M., Lewis, J. A., & Wood, R. J. (2016). An integrated design and fabrication strategy for entirely soft, autonomous robots. *Nature, 536*(7617), 451–455. https://doi.org/10.1038/nature19100
9. Calisti, M., Giorelli, M., Levy, G., Mazzolai, B., Hochner, B., Laschi, C., & Dario, P. (2011). An octopus-bioinspired solution to movement and manipulation for soft robots. *Bioinspiration and Biomimetics*. https://doi.org/10.1088/1748-3182/6/3/036002
10. Ramezani, A., Chung, S. J., & Hutchinson, S. (2017). A biomimetic robotic platform to study flight specializations of bats. *Science Robotics*, *2* (3), eaal2505. https://doi.org/10.1126/scirobotics.aal2505
11. Calisti, M., Picardi, G., & Laschi, C. (2017). Fundamentals of soft robot locomotion. *Journal of the Royal Society Interface*, *14* (130), 20170101. https://doi.org/10.1098/rsif.2017.0101
12. Marchese, A. D., Onal, C. D., & Rus, D. (2014). Autonomous soft robotic fish capable of escape maneuvers using fluidic elastomer actuators. *Soft Robotics, 1*(1), 75–87. https://doi.org/10.1089/soro.2013.0009
13. Marchese, A. D., Katzschmann, R. K., & Rus, D. (2015). A recipe for soft fluidic elastomer robots. *Soft Robotics, 2*(1), 7–25. https://doi.org/10.1089/soro.2014.0022
14. Shintake, J., Rosset, S., Schubert, B., Mintchev, S., Floreano, D., & Shea, H. R. (2015). DEA for soft robotics: 1-gram actuator picks up a 60-gram egg. In *Electroactive polymer actuators and devices (EAPAD)* (Vol. 9430, p. 94301S). https://doi.org/10.1117/12.2084043
15. Youn, J. H., Jeong, S. M., Hwang, G., Kim, H., Hyeon, K., Park, J., & Kyung, K. (2020). Dielectric elastomer actuator for soft robotics applications and challenges. *Applied Sciences*, *10* (2), 640. https://doi.org/10.3390/app10020640
16. Shintake, J., Schubert, B., Rosset, S., Shea, H., & Floreano, D. (2015). Variable stiffness actuator for soft robotics using dielectric elastomer and low-melting-point alloy. In *IEEE international conference on intelligent robots and systems* (Vol. 2015-Decem, pp. 1097–1102). https://doi.org/10.1109/IROS.2015.7353507
17. Henke, E.-F.M., Schlatter, S., & Anderson, I. A. (2017). Soft dielectric elastomer oscillators driving bioinspired robots. *Soft Robotics, 4*(4), 353–366. https://doi.org/10.1089/soro.2017.0022
18. Stokes, A. A., Shepherd, R. F., Morin, S. A., Ilievski, F., & Whitesides, G. M. (2014). A hybrid combining hard and soft robots. *Soft Robotics, 1*(1), 70–74. https://doi.org/10.1089/soro.2013.0002

19. Mosadegh, B., Polygerinos, P., Keplinger, C., Wennstedt, S., Shephard, R. F., Gupta, U., Shim, J., Bertoldi, K., Walsh, C. J., & Whitesides, G. M. (2014). Pneumatic networks for soft robotics that actuate rapidly. *Advanced Functional Materials, 24*(15), 2163–2170. https://doi.org/10.1002/adfm.201303288
20. Yao, L., Niiyama, R., Ou, J., Follmer, S., Della Silva, C., & Ishii, H. (2013). PneUI: Pneumatically actuated soft composite materials for shape changing interfaces. In *UIST 2013—Proceedings of the 26th annual ACM symposium on user interface software and technology*, *Saint Andrews, Scotland, United Kingdom* (pp. 13–22). https://doi.org/10.1145/2501988.2502037
21. Wang, Z., Hang, G., Li, J., Wang, Y., & Xiao, K. (2008). A micro-robot fish with embedded SMA wire actuated flexible biomimetic fin. *Sensors Actuators, A Physics, 144*(2), 354–360. https://doi.org/10.1016/j.sna.2008.02.013
22. Song, G., Kelly, B., & Agrawal, B. N. (2000). Active position control of a shape memory alloy wire actuated composite beam. *Smart Materials and Structures, 9*(5), 711–716. https://doi.org/10.1088/0964-1726/9/5/316
23. Vikas, V., Cohen, E., Grassi, R., Sozer, C., & Trimmer, B. (2016). Design and locomotion control of a soft robot using friction manipulation and motor-tendon actuation. *IEEE Transactions on Robotics, 32*(4), 949–959. https://doi.org/10.1109/TRO.2016.2588888
24. Asif, A., Park, S. H., Soomro, A. M., Khalid, M. A., Salih, A. R. C., Kang, B., Faheem, A., Kim, K. H., & Choi, K. H. (2021). Microphysiological system with continuous analysis of albumin for hepatotoxicity modeling and drug screening. *Journal of Industrial and Engineering Chemistry, 98*, 318–326. https://doi.org/10.1016/j.jiec.2021.03.035
25. Shintake, J., Shea, H., & Floreano, D. (2016). Biomimetic underwater robots based on dielectric elastomer actuators. In *IEEE international workshop on intelligent robots and systems* (Vol. 2016-Novem, pp. 4957–4962). https://doi.org/10.1109/IROS.2016.7759728
26. Jeong, J., Hyeon, K., Han, J., Park, C. H., Ahn, S. Y., Bok, S. K., & Kyung, K.-U. (2021). Wrist assisting soft wearable robot with stretchable coolant vessel integrated SMA muscle. *IEEE/ASME Transactions on Mechatronics*. https://doi.org/10.1109/TMECH.2021.3078472
27. Christianson, C., Goldberg, N. N., Deheyn, D. D., Cai, S., & Tolley, M. T. (2018). Translucent soft robots driven by frameless fluid electrode dielectric elastomer actuators. *Science Robotics, 3*(17), 1–9. https://doi.org/10.1126/SCIROBOTICS.AAT1893
28. Du, T., Hughes, J., Wah, S., Matusik, W., & Rus, D. (2021). Underwater soft robot modeling and control with differentiable simulation. *IEEE Robotics Automation Letters, 6*(3), 4994–5001. https://doi.org/10.1109/LRA.2021.3070305
29. Abbaszadeh, S., Leidhold, R., & Hoerner, S. (2022). A design concept and kinematic model for a soft aquatic robot with complex bio-mimicking motion. *Journal of Bionic Engineering, 19*(1), 16–28. https://doi.org/10.1007/S42235-021-00126-4/FIGURES/7
30. Zhu, Y. Q., Liu, Y. H., Wang, S. X., Zhang, L. H., & Wang, Y. H. (2021). A bionic flexible-bodied underwater glider with neutral buoyancy. *Journal of Bionic Engineering, 18*(5), 1073–1085. https://doi.org/10.1007/S42235-021-00087-8/TABLES/4
31. Witt, W. C., Wen, L., & Lauder, G. V. (2015). Hydrodynamics of C-start escape responses of fish as studied with simple physical models. *Integrative and Computational Biology, 55*(4), 728–739. https://doi.org/10.1093/icb/icv016
32. Katzschmann, R. K., DelPreto, J., MacCurdy, R., & Rus, D. (2018). Exploration of underwater life with an acoustically controlled soft robotic fish. *Science Robotics, 3*(16), 1–13. https://doi.org/10.1126/SCIROBOTICS.AAR3449
33. Cianchetti, M., Calisti, M., Margheri, L., Kuba, M., & Laschi, C. (2015). Bioinspired locomotion and grasping in water: The soft eight-arm OCTOPUS robot. *Bioinspiration and Biomimetics, 10*(3), 1–19. https://doi.org/10.1088/1748-3190/10/3/035003
34. Cianchetti, M., Licofonte, A., Follador, M., Rogai, F., & Laschi, C. (2014). Bioinspired soft actuation system using shape memory alloys. *Actuators, 3*(3), 226–244. https://doi.org/10.3390/act3030226
35. "Ecoflex™ Series—super soft silicone rubber.
36. Quintanar-Guzmán, S., Kannan, S., Olivares-Mendez, M. A., & Voos, H. (2016). Lightweight robotic arm actuated by shape memory alloy (SMA) wires. In *Proceedings 8th international conference on electronics, computers and artificial intelligence (ECAI), Pitesti, Romanica* (pp. 226–244). https://doi.org/10.1109/ECAI.2016.7861065
37. Joyee, E. B., & Pan, Y. (2019). A fully three-dimensional printed inchworm-inspired soft robot with magnetic actuation. *Soft Robotics, 6*(3), 333–345. https://doi.org/10.1089/soro.2018.0082
38. Shah, I., Aziz, S., Soomro, A. M., Kim, K., Kim, S. W., & Choi, K. H. (2020). Numerical and experimental investigation of Y-shaped micromixers with mixing units based on cantor fractal structure for biodiesel applications. *Microsystem Technologies, 27*(5), 2203–2216. https://doi.org/10.1007/S00542-020-05036-9
39. Shah, I., Su Jeon, H., Ali, M., Yang, D. H., & Choi, K. H. (2019). Optimal parametric mixing analysis of active and passive micromixers using Taguchi method. *Journal of Process Mechanical Engineering, 233*(6), 1292–1303. https://doi.org/10.1177/0954408919862997
40. Kim, K., Shah, I., Ali, M., Aziz, S., Khalid, M. A., Kim, Y. S., & Choi, K. H. (2019). Experimental and numerical analysis of three Y-shaped split and recombination micromixers based on cantor fractal structures. *Microsystem Technologies, 26*(6), 1783–1796. https://doi.org/10.1007/S00542-019-04724-5
41. Li, X., Tiong, A. M. H., Cao, L., Lai, W., Phan, P. T., & Phee, S. J. (2019). Deep learning for haptic feedback of flexible endoscopic robot without prior knowledge on sheath configuration. *International Journal of Mechanical Sciences, 163*, 105129. https://doi.org/10.1016/J.IJMECSCI.2019.105129
42. Zhong, G. L., Dou, W. Q., Zhang, X. C., & Yi, H. D. (2021). Bending analysis and contact force modeling of soft pneumatic actuators with pleated structures. *International Journal of Mechanical Sciences, 193*, 106150. https://doi.org/10.1016/J.IJMECSCI.2020.106150
43. Hošovský, A., Piteľ, J., Židek, K., Tóthová, M., Sárosi, J., & Cveticanin, L. (2016). Dynamic characterization and simulation of two-link soft robot arm with pneumatic muscles. *Mechanism and Machine Theory, 103*, 98–116. https://doi.org/10.1016/j.mechmachtheory.2016.04.013
44. Duriez, C., & Bieze, T. (2017). Soft robot modeling, simulation and control in real-time. *Biosystems and Biorobotics, 17*, 103–109. https://doi.org/10.1007/978-3-319-46460-2_13
45. Sreekumar, M., Nagarajan, T., Singaperumal, M., Zoppi, M., & Molfino, R. (2007). Critical review of current trends in shape memory alloy actuators for intelligent robots. *Industrial Robot, 34*(4), 285–294. https://doi.org/10.1108/01439910710749609
46. Jonnalagadda, K., Kline, G. E., & Sottos, N. R. (1997). Local displacements and load transfer in shape memory alloy composites. *Experimental Mechanics, 37*(1), 78–86. https://doi.org/10.1007/BF02328753
47. Llewellyn-Evans, H., Griffiths, C. A., & Fahmy, A. A. (2020). An experimental study into displacement of a shape memory alloy actuated robotic microgripper. *Engineering Research. Express, 2*(1), 015027. https://doi.org/10.1088/2631-8695/ab6d27